EAI Endorsed Transactions
on Energy Web
Research Article EAI.EU

Research on Electromagnetic-Thermal-Mechanical Multiphysics Coupling Simulation Analysis of Converter Transformers

Zhichuang Li[1a], Tan Li[1b], Yongfan Guo[1c], Shenghui Wang[2*]

[1]State Grid Economic and Technological Research Institute Co., Ltd, Beijing 102209, China
[2]School of Electrical and Electronic Engineering, North China Electric Power University, Beijing 102206, China

Abstract

Addressing the limitations of conventional single-physics analysis methods in accurately revealing the internal electro-thermal-mechanical interaction mechanisms, this study established a fully coupled electro-magnetic-thermal-mechanical model for converter transformer windings. This model comprehensively accounts for the effects of harmonic currents and DC bias, employing bidirectional coupling calculations to elucidate the complete propagation process from electromagnetic losses to temperature distribution and structural stresses. Simulation results indicate that harmonic losses constitute the primary factor driving localised hotspot temperature rise. The resulting non-uniform thermal expansion, coupled with electromagnetic forces, generates significant stress concentrations in regions such as the winding ends.

Keywords: Converter transformer; Multiphysics coupling; Harmonic currents; DC bias; Hotspot temperature rise

Received on 04 November 2025, accepted on 21 December 2025, published on 22 April 2026

doi: 10.4108/ew.12727

1. Introduction

Against the backdrop of the dual carbon strategy objectives and the development of new power systems, the power source structure and load characteristics of the grid are undergoing profound changes. The large-scale grid integration of intermittent renewable energy sources such as wind and solar power, coupled with the widespread application of various power electronic devices, has significantly increased harmonic content within the grid. These places heightened demands on the safe and stable operation of converter transformers [1-2]. As a critical main equipment within ultra-high voltage direct current transmission systems, converter transformers serve alongside converters as pivotal interfaces between AC and DC systems, facilitating AC-DC conversion on both rectifier and inverter sides. Their operational status directly determines the safety and stability of the entire DC transmission system [3], while also carrying the risk of DC bias induced by geomagnetic currents [4]. The combined effects of complex electrical operating conditions and thermal stresses render the multi-physics coupling phenomena within converter transformers exceptionally intricate and severe. Conventional design and analysis methods, based on single-physics fields or empirical formulas, are increasingly inadequate for meeting the urgent demands of precise condition assessment and safe operation and maintenance [5].

Research on converter transformers is primarily divided into experimental investigations based on sensor deployment and numerical simulation studies. Regarding experimental research, Abdali et al. [6] conducted an experimental case study on oil-immersed distribution transformers, proposing a novel method for hotspot temperature prediction to enhance thermal monitoring capabilities. Jin et al. [7] focused on the structural innovation of magnetic components, designing a

[a]lizhichuang@chinasperi.sgcc.com.cn,
[b]litan@chinasperi.sgcc.com.cn, [c]progyf@126.com,
[*]shm_020226@126.com

high-efficiency three-phase integrated transformer for resonant converters and validating its high-density performance through hardware experiments. Furthermore, Duan et al. [8] investigated the propagation law of partial discharge ultrasonic signals specifically within converter transformers, providing valuable data for internal fault detection. However, experimental data measurement is often not comprehensive, making it difficult to obtain a clear understanding of the overall state of the transformer; numerical simulation can effectively fill these gaps in data measurement.

In the field of simulation research, numerical methods have proven essential for both control strategy optimization and internal physical field analysis. Jin et al. [9] utilized simulation techniques to conduct multi-objective optimization for dual active bridge converters, demonstrating the efficacy of numerical approaches in handling complex variable-frequency modulation strategies. Regarding the internal physics of transformers, Liu et al. [10] specifically investigated the impact of high-proportion harmonic currents on ultra-high voltage (UHV) converter transformers, clarifying the distribution laws of magnetic fields, losses, and temperature under distorted load conditions. Zhang Jun et al. [11] performed detailed three-dimensional simulations of temperature and flow fields within dry-type European transformers, systematically analyzing airflow paths and thermal efficiency under various fan configurations and ventilation port layouts. This work provides critical insights for optimizing heat dissipation designs. The work of Wang Yuan et al. [12] revealed inherent limitations in two-dimensional axisymmetric models when simulating transformer winding temperature rise: by neglecting tangential oil flow in three-dimensional space, their predictions systematically overestimate the scale of 'oil flow dead zones' and hotspot temperatures. Additionally, Yang Fan et al. [13] established an electromagnetically-mechanically coupled model accounting for material nonlinearities, elucidating the dynamic evolution of mechanical states and cumulative damage mechanisms in transformer windings subjected to multiple short-circuit impacts.

Despite significant advances in multiphysics simulation, many electromagnetic-mechanical coupling analyses overlook steady-state thermal stresses induced by non-uniform temperature rise during long-term operation and their combined effects with electromagnetic forces. This leads to inaccuracies in predicting local overheating and mechanical deformation risks. Addressing these research gaps and practical engineering needs, this paper establishes a high-precision, fully coupled 'electromagnetic-thermal-mechanical' simulation model for converter transformer windings. This model enables comprehensive calculation of temperature, deformation, and stress distributions under complex operating conditions, thereby providing more reliable theoretical support for optimizing converter transformer design and implementing fault early warning systems. The specific workflow is as follows: First, a three-dimensional geometric model is established and meshed. Next, boundary conditions are set, incorporating external circuit excitation—comprising higher harmonics and DC components—into the coil within the electromagnetic field module. A transient solver then calculates the electromagnetic loss distribution and electromagnetic force density within the winding. Subsequently, the electromagnetic losses are imported as heat sources into the thermal field module. Coupling with the laminar flow module enables coupled flow-heat transfer calculations to determine temperature distributions and thermal stress distributions. Finally, both the thermal stress generated by the temperature field and the electromagnetic forces produced by the electromagnetic field are simultaneously introduced into the solid mechanics module. The transient solver then calculates the displacement and deformation of the windings and core.

2. Algorithm Analysis and Mathematical Modelling

2.1. Multiphysics simulation equations

2.1.1 Electromagnetic field equations

Electromagnetic field analysis serves as the starting point for coupled simulations, with its governing equations based upon Maxwell's equations. Under the magnetostatic assumption, which neglects displacement currents, the governing equations may be simplified to:

$$\nabla \cdot H = J \tag{1}$$

$$\nabla \cdot E = -\frac{\partial B}{\partial t} \tag{2}$$

$$E = -\frac{\partial A}{\partial t} \tag{3}$$

Where the magnetic field strength H is measured in A/m, the total current density J in A/m², the electric field strength E in V/m, and the magnetic flux density B in T. The constitutive relationship for the iron core is:

$$B = f\left(||H||\right)\frac{H}{||H||} \tag{4}$$

$$J = \sigma_e E \tag{5}$$

$$D = \varepsilon_0 \varepsilon_r E \tag{6}$$

Where σ_e denotes electrical conductivity in S/m, D denotes electric flux density in C/m², ε_0 denotes the vacuum permittivity in F/m, and ε_r denotes the relative permittivity as a dimensionless quantity. The constitutive relationship for air is:

$$B = \mu_0 \mu_r H \tag{7}$$

The vacuum permeability μ_0 is expressed in units of H/m, while the relative permeability μ_r is a dimensionless quantity.

2.1.2. Equations of heat transfer in solids and fluids

1. Equations of Fluid Mechanics

Within converter oil transformers, the flow of insulating oil is typically governed by the Navier-Stokes equations. For laminar flow, COMSOL solves the equations of mass conservation and momentum conservation. The momentum conservation equation is the fundamental equation describing fluid motion:

$$\rho \frac{\partial u}{\partial t} + \rho(u \cdot \nabla)u = \nabla \cdot [-pI + K] + F \tag{8}$$

Where the fluid density ρ is in kg/m³, the velocity vector field u is in m/s, the fluid pressure p is in N/m², the unit matrix I is dimensionless, the viscous stress tensor K is in N/m², and the volumetric force F is in N/m³.

For weakly compressible fluids, the mass conservation equation holds:

$$\nabla \cdot (\rho u) = 0 \tag{9}$$

2. Equations of Heat Transfer in Solids and Fluids

The energy conservation equation is employed to determine the distribution of the temperature field. The general form of the energy equation is:

$$\rho C_p \frac{\partial T}{\partial t} + \nabla \cdot q + \rho C_p u \cdot \nabla T = Q \tag{10}$$

According to Fourier's law of heat conduction:

$$q = -k\nabla T \tag{11}$$

Here, the fluid density ρ is expressed in kg/m³, the specific heat capacity at constant pressure C_p in J/(kg·K), the temperature T in K, the velocity vector field u in m/s, the heat generated per unit volume Q in W/m³, and the thermal conductivity k in W/(m·K). Within the core and windings, velocity u=0, thus eliminating the convective term and simplifying the equation to a pure heat conduction equation:

$$\rho C_p \frac{\partial T}{\partial t} + \nabla \cdot (-k\nabla T) = Q_{heat} \tag{12}$$

Among these, the electromagnetic loss Q_{heat} of the transformer originates from the electromagnetic heat density calculated via electromagnetic field simulation, expressed in units of W/m³.

3. Equations of Solid Mechanics

The Solid Mechanics interface primarily calculates the deformation, stresses, and vibrations of windings subjected to electromagnetic forces and thermal expansion. The equations of motion form the core equations of solid mechanics, constituting a transient dynamic problem when windings experience time-varying electromagnetic forces. The equilibrium equations are:

$$0 = \nabla \cdot S + F_v \tag{13}$$

Herein, the stress tensor S is expressed in Pa, and the volumetric load vector F_v is expressed in N/m³.

Linear elastic materials constitute the core mathematical model describing how materials deform under stress and how thermal expansion effects are superimposed. Their constitutive relationship is:

$$S = S_{ad} + C : \varepsilon_{el} \tag{14}$$

$$\varepsilon_{el} = \varepsilon - \varepsilon_{inel} \tag{15}$$

Where the additional stress S_{ad} is expressed in Pa, the elastic stiffness tensor C is expressed in Pa, and the elastic strain ε_{el} represents the recoverable portion of deformation in the material, being a dimensionless quantity. ε denotes the total strain, while ε_{inel} denotes the inelastic strain.

To prevent loosening or deformation under short-circuit electrodynamic forces, the upper and lower ends of the windings are firmly clamped by pressure plates and tie rods. The stresses acting on the converter transformer core and windings can be decomposed as follows:

$$S_{ad} = S_0 + S_{ext} + S_q \tag{16}$$

Where S_0 denotes the initial stress, S_{ext} represents the external stress, and S_q signifies the viscoelastic stress, with all stresses expressed in Pa.

The displacement phenomena arising from stresses applied to the converter winding and core must be accounted for to ensure that overall winding oscillation caused by electromagnetic forces does not induce stress. Stress shall only occur when the winding undergoes bending or compression. Under the assumption of small deformations, the strain equation is incorporated as follows:

$$\varepsilon = \frac{1}{2}[(\nabla u)^T + \nabla u] \tag{17}$$

Herein, the displacement vector u is expressed in metres.

2.2 Converting the physical model

The prototype converter transformer studied herein is the 297.5 MVA/500 kV single-phase double-winding converter transformer from the Sanchang Longquan converter station. The model of the ±500 kV converter transformer is shown in Figure 1:

Figure 1. Converter Transformer Physical Model

The structural parameters of the converter transformer are as shown in Table 1:

Table 1. Structure Parameters of Converter Transformer

Structure	Dimensions (mm)
fuel tank	4500*2000*2500
Window height	1200
iron yoke	4000*800*2200
Centre distance between columns	1405
Number of turns in the grid-side winding	867
Valve-side winding turns	452
Inner diameter of grid-side winding	800
Grid-side winding outer diameter	908
Inner diameter of valve-side winding	1000
Valve-side winding outer diameter	1182

The simulation process requires material filling of the entire converter transformer assembly, comprising primarily the core, windings, transformer oil, and tank. Key material parameters for filling are detailed in Table 2.

Table 2. Converter Transformer Material Parameters

	Relative magnetic permeability	Relative permittivity	Density (kg/m³)	Electrical conductivity (S/m)
winding	1	1	8960	5.99*107
Transformer oil	1	2.2	880	0.10
Iron core	8000	1	7870	1.00*107
fuel tank	4000	1	7870	1.12*107

3. Modelling and Meshing

3.1. Simplified model

Owing to the exceptionally intricate physical structure of converter transformers, which incorporate tens of thousands of laminated silicon steel sheets and multi-layered insulated coil windings, constructing a full-scale three-dimensional model encompassing all geometric details within multi-physics simulations would result in an exponential increase in finite element mesh count. This would not only cause computer memory overflow and significantly reduce computational efficiency, but also make the non-linear coupled solution process difficult to converge. To strike a balance between computational accuracy and computational resources, the geometric model of the converter transformer underwent reasonable simplification and homogenisation. The simplified model is shown in Figure 2.

The model primarily consists of the core, windings, tank, and insulating oil fluid domain. The specific simplification process is as follows:

1) Equivalent treatment of the core model: The densely laminated silicon steel sheet structure of the core is simplified into a macroscopically continuous solid geometry. To preserve the laminated structure's guiding effect on magnetic paths and its magnetic resistance characteristics, the model does not physically depict each individual silicon steel sheet layer. Instead, through material property definitions, these are set as equivalent physical layers possessing anisotropic magnetic permeability.

2) Homogenisation of the winding model: The converter transformer windings comprise grid-side windings, valve-side windings, and voltage-regulating windings. As the voltage-regulating windings do not participate in excitation under specific simulation conditions, their contribution to the main leakage magnetic field and temperature rise distribution is negligible. Therefore, to simplify the topology, the voltage-regulating windings are omitted from the model. For grid-side and valve-side windings, individual copper conductors and inter-turn insulation are not depicted separately. Instead, a 'macroscopic equivalent ring-shaped body' is employed as a substitute. Based on the principle of ampere-turn balance, uniform equivalent current density is applied across the cross-section of the ring-shaped body to simulate the electromagnetic excitation generated by the actual multi-turn coil.

3) Oil Tank and Fluid Domain: The oil tank is simplified to an outer thin-walled rectangular prism boundary, omitting minor components such as stiffeners, radiator interfaces, and complex lead supports that exert negligible influence on the overall field. Transformer oil fills the void between the core, windings, and tank, forming a continuous fluid heat transfer domain.

Through these simplifications, the model eliminates non-critical geometric features while retaining the core structures governing the electromagnetic-thermal-mechanical coupling mechanisms. This approach satisfies the accuracy requirements for finite element simulation whilst significantly enhancing computational speed.

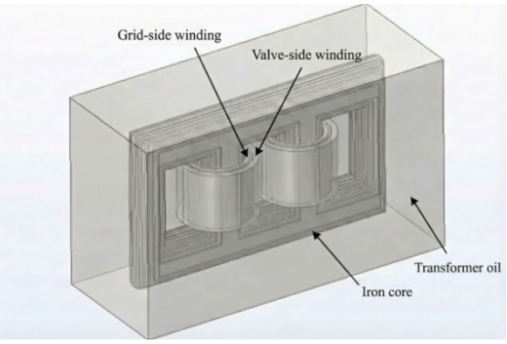

Figure 2. Simplified Model of a Converter Transformer

3.2. Meshing

To balance the accuracy and efficiency of the model solution, the model was subdivided into regional meshes. The winding section employed triangular meshes on the end faces with axial sweeping. Due to the thickness constraints of the silicon steel laminations, the core section utilised a finer tetrahedral mesh. The entire external iron shell was also subdivided using tetrahedral meshes. The mesh subdivision diagram is shown in Figure 3.

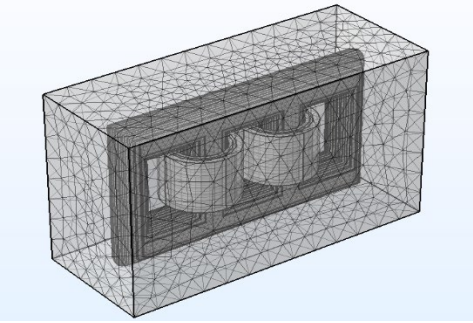

Figure 3. Converter Transformer Mesh Partition Diagram.

3.3. Simulation boundary condition

3.3.1. Electromagnetic field boundary conditions and excitation

The external circuit on the grid side of the converter employs an AC power supply, with the circuit parameters set as shown in Table 3.

Table 3. Circuit Parameter Settings

Name	Parameters
Voltage (kV)	500
***Valve-side resistance* (Ω)**	0.89
***Grid-side resistance* (Ω)**	2.2
***Frequency* (Hz)**	50

The voltage and current waveforms on both sides are shown in Figures 4 and 5. Figure 4 illustrates the waveforms of voltage over time for the grid-side and valve-side windings of the converter transformer during start-up or transient processes. As illustrated, the grid-side winding voltage exhibits a standard sinusoidal alternating waveform at a frequency of 50Hz. Figure 5 presents the time-domain current waveforms for both the grid-side and valve-side windings of the converter transformer under steady-state operating conditions. Both current waveforms display highly regular sinusoidal characteristics at a fundamental frequency of 50Hz.

Magnetic insulation: The outer surface of the tank and the far-field air domain are set as magnetically insulated (n×A=0). Core laminations equivalent: Anisotropic relative permeability (radial μr=1000, interlayer μr=20) is employed to simulate the lamination effect. Coils employ solid materials, with wire models utilising uniform multi-turn configurations. Coil type is selected numerically, while coil excitation employs circuit (current) coupling of circuit modules. The magnetisation model utilises relative permeability, and the dielectric model employs relative permittivity. The input surface for coil excitation is illustrated in Figure 6.

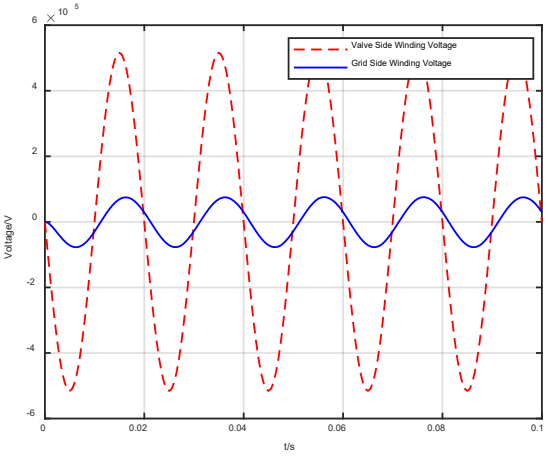

Figure 4. Voltage Waveform Diagram

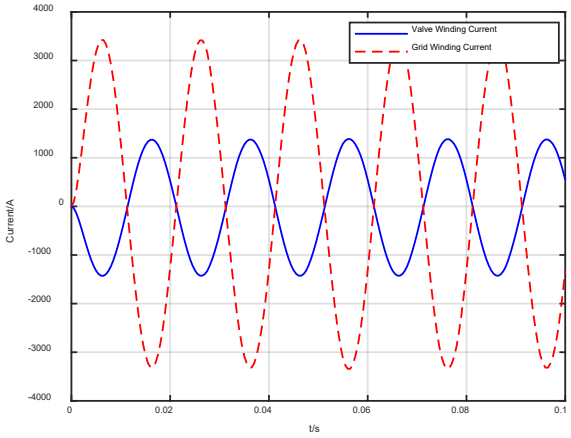

Figure 5. Current waveform diagram

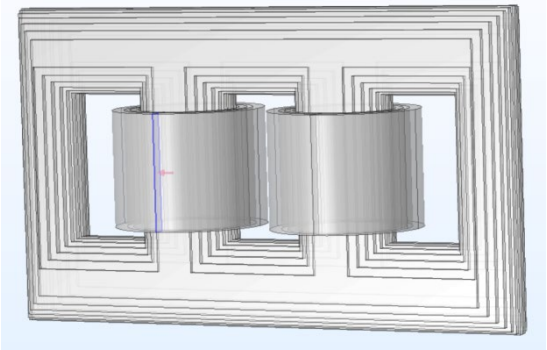

Figure 6. Input surface for coil excitation

3.1.2. Boundary conditions for temperature and flow fields

The primary heat sources required for the temperature field analysis stem from the losses within the converter transformer's core and windings. The core's heating arises from no-load losses, with its heat flux density calculated as the no-load loss divided by the volume. The windings' heating originates from load losses, with the high- and low-voltage heat flux densities determined as the load loss divided by the respective volume. Parameters are detailed in Table 4. The converter transformer oil is defined as a fluid domain, while the core and windings are designated as solid domains. Convective heat flux is applied to the transformer casing to describe convective heat transfer between the fluid and solid surfaces, with the iron heat transfer coefficient typically ranging between 10 and 16 W/m²•K. The heat flux type on the outer wall of the oil tank is set as convective heat flux. The top surface exhibits a turbulent flow layer, the side surfaces boundary layer flow, and the bottom surface stagnant flow layer. Consequently, the heat transfer coefficients differ: the bottom surface is set at 10 W/m²•K, the side surfaces at 16 W/m²•K, and the top surface at 14 W/m²•K. The initial temperature is set at 20°C.

Table 4. Thermal loss rate of the core and windings

Region	Total loss (kW)	Volume (m^3)	Heat dissipation rate (W/m^3)
Iron core	20	2.21	9050
Valve-side winding	120	0.636	188679
Grid-side winding	80	0.404	198020

For the fluid domain, it is assumed that the transformer oil is initially at rest. The model accounts for the effects of gravity on oil flow and natural convective heat transfer, hence defining a gravitational acceleration of 9.8 m/s^2 along the positive Z-axis direction. Furthermore, to address numerical convergence difficulties arising from variations in liquid column height within the gravitational field for incompressible fluids, this model incorporates a hydrostatic pressure compensation approximation algorithm. This method significantly enhances computational efficiency and solution stability while maintaining computational accuracy.

On a computer equipped with an Intel Core i5-9300H processor, 4 cores, 2.40 GHz, and 16 GB of memory, the fully coupled transient simulation of electrical-magnetic-thermal-mechanical interactions established in this paper employs a physically controlled mesh with extreme refinement. This includes a winding sweep combined with a tetrahedral mesh for the core, resulting in approximately 400,000 total degrees of freedom. The duration of a single complete computational run is as shown in Table 5:

Table 5. Time consumption at different computational stages

Computational phase	Solver type	time-consuming
Frequency domain electromagnetic field (including harmonics and DC bias)	MUMPS Direct Solver	10 min
Transient electromagnetic field (0–0.1 s, 2 ms step size)	PARDISO + Time-Dependent	1 h 7 min
Flow-heat coupling steady state (up to 19,000 s)	Fully Coupled + Boussinesq	3 h 57 min
Transient Solid Mechanics	Dynamic Implicit + Thermal Expansion Coupling	1 h 24 min
Total time taken		6 h 38 min

3.1.3. Boundary conditions for solid mechanics

Within the Solid Mechanics Module, to reflect the stress and constraint conditions of the converter transformer, the model incorporates the following boundary conditions and loads: A volume load is applied to the winding domain, incorporating the Lorentz force density calculated via the electromagnetic field interface as a source term within the volume load. This achieves strong unidirectional coupling between the electromagnetic and mechanical fields. For constraint conditions, the core base and tank bottom are fixed to simulate the transformer's installation on a rigid foundation. To model the mechanical clamping of internal clamps and pressure plates, roller supports with specified displacement conditions are applied to the core sides and winding ends. This restricts normal rigid-body displacement while permitting free tangential sliding, thereby accommodating thermal expansion-induced deformation.

4. Analysis of Results

4.1. Magnetic field analysis

Based on the electromagnetic field control equations and the nonlinear material constitutive model established earlier, numerical calculations were performed on the transient magnetic field of the converter transformer under the combined effects of DC bias and harmonic currents.

Figures 7 and 8 illustrate the distribution of magnetic flux density magnitude and magnetic flux paths in the core and winding regions of the converter transformer at different simulation time points.

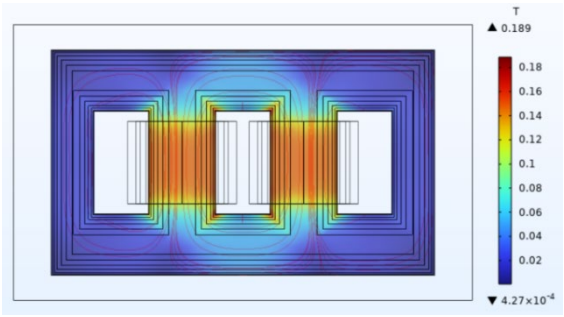

Figure 7. Magnetic flux density modulus at time T=0.0015s

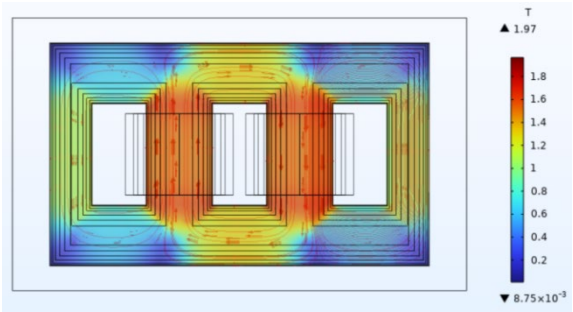

Figure 8. Magnetic flux density modulus at time T=0.0095s

The results indicate that the magnetic flux density distribution within the core exhibits time-varying nonlinear characteristics. Over a single power frequency cycle, the maximum local magnetic flux density within the core fluctuates between 0.189 T and 1.97 T. Notably, the peak

value of 1.97 T exceeds the saturation inflection point of conventional silicon steel sheets, which is approximately 1.7 T, indicating that the core enters the saturation region at specific phases. This finding quantitatively demonstrates that under DC bias conditions, the superimposed DC component elevates the core's operational magnetic flux density significantly above the design value for conventional AC operation. This periodically varying state of magnetic saturation and leakage flux distribution alters both the internal loss distribution and stress state within the transformer, thereby defining the initial load conditions for subsequent electromagnetic loss calculations and structural mechanical analyses.

4.2. Thermal field analysis

The electromagnetic loss density distribution obtained from the aforementioned electromagnetic field simulation calculations (including winding Joule losses, core hysteresis losses, and eddy current losses) was mapped as volumetric heat sources into the temperature field model. Through fluid-thermal conduction two-way coupling solution, the steady-state temperature distribution of the converter transformer under DC bias conditions was obtained.

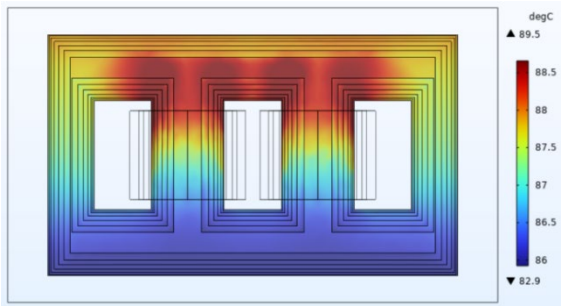

Figure 9. Temperature distribution of the iron core

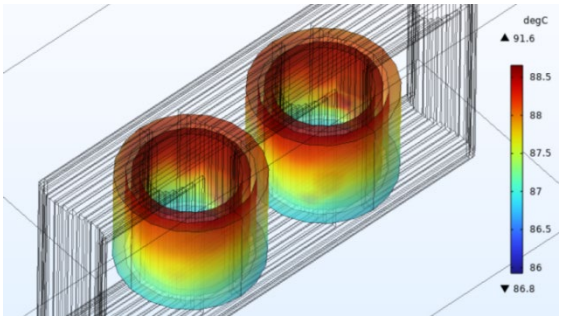

Figure 10. Temperature distribution of the winding

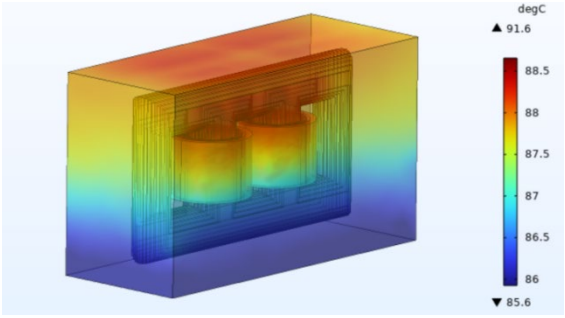

Figure 11. Temperature distribution of the fuel tank

Figures 9 to 11 present the three-dimensional overall and two-dimensional cross-sectional temperature distribution contour plots of the transformer at t=19000s during simulation. From the global thermal field distribution characteristics, the transformer interior exhibits a pronounced vertical temperature gradient, with an overall distribution pattern of 'lower temperatures at the bottom and higher temperatures at the top'. As illustrated, the lowest temperature of the insulating oil is approximately 85.6°C, primarily distributed at the bottom of the tank. Conversely, high-temperature zones are concentrated in the upper regions of the windings and core.

The windings constitute the primary heat-generating and high-temperature concentration components, with the highest temperature reaching 91.6°C. Hotspots are not uniformly distributed but are concentrated at the uppermost end of the windings. Concurrently, the skin effect induced by harmonic currents at the high-voltage terminals further exacerbates localised Joule heating accumulation. By comparison, the core's maximum temperature was approximately 88.9°C, slightly lower than the winding hotspot. The core's high-temperature zone was likewise located at the upper yoke, attributable not only to its internal nonlinear magnetic losses but also to heating from the surrounding rising high-temperature oil flow.

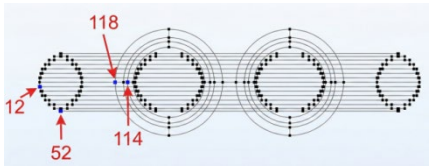

Figure 12. Converter Hotspot Selection

Figure 12 depicts the selected hotspots of the converter transformer, where points numbered 114 and 118 represent the apexes of the grid-side and valve-side windings respectively, while points numbered 12 and 52 denote locations on the core. Figures 13 and 14 present the temperature rise curves for different hotspots at distinct time points. Within the initial 1000 seconds of simulation, the temperature curve exhibits a steep peak followed by a rapid decline. As the system enters a relatively stable operating state with established insulating oil circulation, the winding temperature begins a steady, near-

logarithmic rise. During this phase, heat generated by thermal sources continues to accumulate, yet the rate of temperature increase gradually diminishes, indicating the system is progressively approaching thermal equilibrium. The two curves closely overlap during this phase, indicating that throughout most of the temperature rise process, the radial temperature difference at the top of the windings is minimal. Heat conduction within the copper conductors is sufficiently rapid to achieve temperature uniformity across localised regions. As the simulation approaches 20,000 seconds, the final temperature stabilises at approximately 100℃. This signifies that the heat generation power and the heat dissipation power have reached a dynamic equilibrium. The grid-side winding curve remains slightly elevated relative to the valve-side curve, reflecting localised loss variations attributable to unevenly distributed leakage magnetic fields. This validates that end leakage magnetic effects constitute the primary cause of localised hotspots.

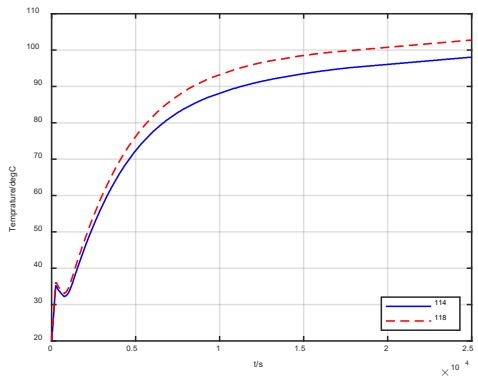

Figure 13. Temperature Rise Curve Diagram for Winding Hotspots

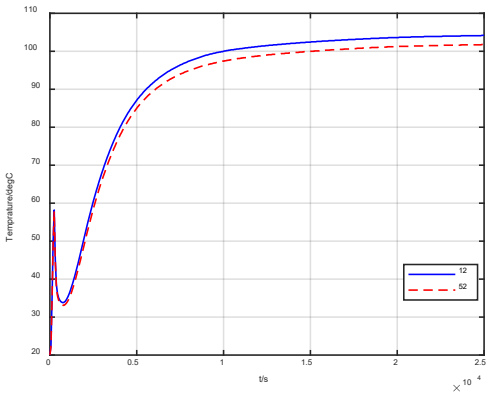

Figure 14. Temperature Rise Curve Diagram for Iron Core Hotspots

4.3. Force field analysis

Based on a multiphysics coupling simulation framework, this section combines the Lorentz force density and core magnetostrictive force derived from electromagnetic field calculations with thermal strain generated from temperature field computations. These are jointly input as volumetric loads into the structural mechanics module to solve for the mechanical deformation and stress characteristics of the converter transformer under DC bias conditions. Figures 15 to 17 display the displacement field distribution contour plots for the entire transformer and its windings at the simulation time t=0.0095s.

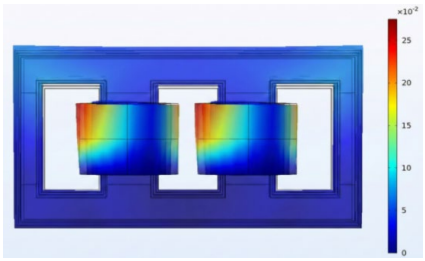

Figure 15. Converter-type mechanical deformation front elevation

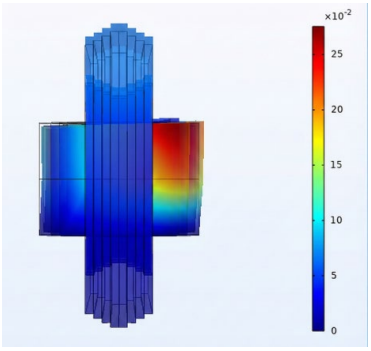

Figure 16. Side View of Mechanical Deformation in Converter Transformation

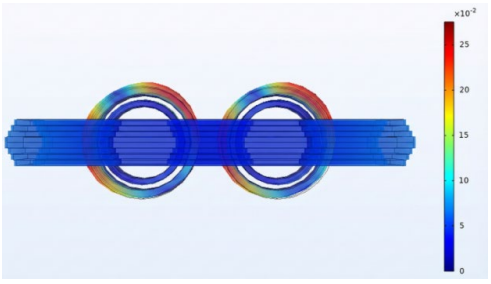

Figure 17. Top view of mechanical deformation conversion

To realistically replicate the actual operating conditions of converter transformers, this study altered the characteristic harmonic content to achieve a harmonic distortion rate of 8.9%. To quantitatively assess the impact of harmonic content on winding end stresses, a comparative operating condition was established: whilst maintaining the DC bias component

unchanged, the harmonic coefficients were proportionally amplified by a factor of 1.1. The resulting mechanical stress views of the converter transformer are depicted in Figures 18 and 19.

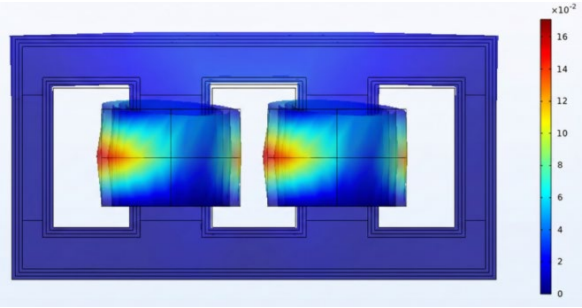

Figure 18. Frontal view of mechanical deformation of the converter transformer at a harmonic distortion rate of 8.9%

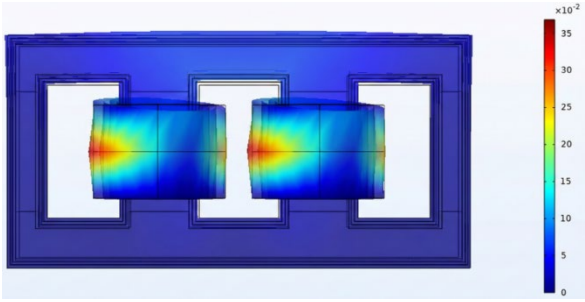

Figure 19. Frontal view of mechanical deformation in converter transformers with a 10% increase in harmonic content

Analysis of the spatial distribution characteristics of the overall displacement field indicates that mechanical deformation is primarily concentrated in the relatively low-stiffness winding region, whilst the core maintains superior structural stability owing to its higher Young's modulus. Quantitative cloud diagram data indicates that the maximum displacement amplitude in the winding region is approximately 0.28 mm. The top view reveals that the valve-side windings exhibit an outward expansion tendency under electromagnetic force, with deformation amplitude significantly greater than that of the grid-side windings. Analysis of the side view further shows that displacement in the upper portion of the windings is markedly greater than in the lower portion. This phenomenon exhibits strong correlation with the ‘hot top, cold bottom’ temperature gradient distribution observed in the preceding thermal field analysis. Higher temperatures in the upper copper conductors of the windings induce greater thermal expansion strain. This thermal strain spatially vectorially superimposes with the mechanical strain induced by electromagnetic forces, further amplifying structural displacement at the ends.

Simulation results indicate that harmonic content exerts a significant amplifying effect on end-winding stresses. When neglecting harmonic influences, the maximum axial displacement at the valve-side winding end is 0.28 mm, with a peak stress of 42 MPa. Under rated operating conditions with an 8.9% harmonic distortion rate, the maximum displacement at the valve-side winding end reached 0.30 mm, with a maximum stress of 45 MPa. When the overall harmonic content increased by 10%, the maximum axial displacement at the valve-side winding end rose to 0.32 mm, with a maximum stress of 47 MPa. Compared to the harmonic-free baseline condition, the stress increase in the valve-side winding under high-harmonic conditions was approximately 12%, with displacement increasing by about 14.3%. For the grid-side winding ends, stress increased by 6.8% and displacement by 7.5%, showing consistent overall trends. Both stress and displacement increases slightly exceeded the harmonic content increase ratio, indicating a certain degree of non-linear amplification effect of the additional electromagnetic forces generated by harmonic currents at the winding ends. These results demonstrate that in actual converter transformer operation, even a modest rise in harmonic content can lead to a non-negligible risk of stress accumulation at the mechanically vulnerable winding ends, warranting sufficient attention.

5. Conclusions

This paper addresses the limitation of traditional single-physics analysis methods in accurately revealing the electro-thermal-mechanical interaction mechanisms within converter transformers. It establishes a fully coupled electro-magnetic-thermal-mechanical model for converter transformers that comprehensively accounts for the effects of harmonic currents and DC bias. The principal conclusions are as follows:

1) A fully coupled multiphysics simulation model for converter transformers has been established. Based on equivalent medium theory, a three-dimensional finite element model incorporating external circuit excitation was developed. Through bidirectional data transfer between electromagnetic losses, fluid-thermal conjugate heat transfer, and structural mechanics, high-precision fully coupled solutions for steady-state operational characteristics under DC bias conditions were achieved.

2) The simulation revealed the non-uniform temperature rise distribution pattern caused by magnetic saturation. Results confirmed that DC bias induced peak magnetic flux densities of 1.97 T in the core, leading to deep saturation and significantly enhanced leakage flux. The resulting combination of end-winding eddy current losses and skin effect induces vertical temperature gradients in the windings, with peak temperatures at the top reaching approximately 100°C. This validates that redistributed leakage flux is the primary cause of localised overheating.

3) The cumulative effect and distribution pattern of harmonic currents on winding end stresses have been revealed. Simulations indicate that mechanical deformation exhibits a spatial characteristic where valve-side stresses exceed grid-

side stresses, and top-side stresses surpass bottom-side stresses. Data indicates that under rated harmonic conditions, end-winding stresses on the valve side reached 45 MPa—an increase of approximately 7.1% compared to non-harmonic conditions. When harmonic content further increased by 10%, stress accumulated to 47 MPa. These findings demonstrate that harmonic presence significantly elevates the stress baseline of windings, where even minor fluctuations amplify fatigue failure risks at mechanically vulnerable points.

References

[1] H. Wang, J. Li, Y. Song, Y. Sun, and H. Wang, "Study on Loss Distribution and Characteristics of Converter Transformers under Fundamental and Harmonic Components," New Technologies in Electrical Engineering and Power, vol. 40, no. 10, pp. 10–17, 2021.

[2] A. Abdali, K. Mazlumi, and A. Rabiee, "Harmonics impact on hotspot temperature increment of distribution transformers: Nonuniform magnetic-thermal approach," International Journal of Electrical Power & Energy Systems, vol. 157, Art. no. 109826, Jun. 2024.

[3] A. Hassankashi, A. Dini, S. Pirouzi, M. Veisi, and M. Bahreini, "Flexible renewable integrated energy system capabilities to improve voltage stability with power quality and economic environmental operation of smart grid," Scientific Reports, vol. 15, no. 1, Art. no. 29052, 2025.

[4] Z. Li, W. Li, Z. Zhang, et al., "Development Strategy of Flexible Resources in China's Power System under the Carbon Peaking and Carbon Neutrality Goals," Strategic Study of CAE, vol. 26, no. 4, pp. 108–120, 2024.

[5] C. Niu, Y. Xu, and X. Fan, "Research on Grid Side Harmonic Suppression Method for Cascaded Power Electronic Transformers Under Unbalanced Grid Conditions," Electrical Measurement & Instrumentation, vol. 61, no. 9, pp. 40–47, 2024.

[6] A. Abdali, A. Abedi, K. Mazlumi, A. Rabiee, and J. M. Guerrero, "Novel hotspot temperature prediction of oil-immersed distribution transformers: An experimental case study," IEEE Transactions on Industrial Electronics, vol. 70, no. 7, pp. 7310–7322, Jul. 2023.

[7] J. F. Jin, A. Nabih, T. L. Yuan, and Q. Li, "A High-Efficiency High-Density Three-Phase CLLC Resonant Converter With a Universally Derived Three-Phase Integrated Transformer for On-Board-Charger Application," IEEE TRANSACTIONS ON POWER ELECTRONICS, vol. 39, no. 4, pp. 4350–4366, 2024.

[8] H. Duan, L. Cheng, C. X. Luo, J. Zhang, and Z. Su, "Research on propagation law of partial discharge ultrasonic signal in converter transformer," AIP ADVANCES, vol. 14, no. 6, Art. no. 065023, Jun. 2024.

[9] H. Jin, Y. Pei, L. Wang, G. Wang, X. Dong and Q. Zhou, "Multiobjective Optimization for Dual Active Bridge Converter Under Variable-Frequency Single-Phase-Shift Modulation," IEEE Transactions on Power Electronics, vol. 41, no. 2, pp. 2685-2702, Feb. 2026.

[10] C. Liu, H. Hao, J. Liao, R. Liao, Y. Fan, W. Li, and Z. Li, "High proportion and large value harmonic current influence on the magnetic field, loss and temperature distribution for ultrahigh voltage converter transformer," IET Electric Power Applications, vol. 18, no. 2, pp. 208–225, Feb. 2024.

[11] J. Zhang, H. Luo, S. Yuan, et al., "Simulation Calculation of Three-Dimensional Temperature Field of European-Style Transformer," Transformer, vol. 62, no. 10, pp. 20–26, 2025.

[12] Y. Wang, Z. Tang, F. Niu, et al., "Three-dimensional simulation calculation and analysis of winding temperature distribution of 220 kV natural ester transformer," Insulating Materials, vol. 58, no. 8, pp. 50–56, 2025.

[13] F. Yang, Z. Liu, J. Jiang, and G. Tan, "Computation of Electromagnetic-Force Coupled Fields and Multi-Parameter Vibration Characteristics of Transformer Windings Under Multiple Short-Circuit Impacts," Transactions of China Electrotechnical Society, pp. 1–16, 2025.